

Cite this: *Dalton Trans.*, 2012, **41**, 1742

www.rsc.org/dalton

PAPER

Synthesis, purification, and characterization of phosphine oxides and their hydrogen peroxide adducts†

Casie R. Hilliard, Nattamai Bhuvanesh, John A. Gladysz and Janet Blümel*

Received 3rd October 2011, Accepted 21st October 2011

DOI: 10.1039/c1dt11863c

Reactions of the tertiary phosphines R_3P ($R = \text{Me, Bu, Oct, Cy, Ph}$) with 35% aqueous H_2O_2 gives the corresponding oxides as the H_2O_2 adducts $R_3P=O \cdot (H_2O_2)_x$ ($x = 0.5-1.0$). Air oxidation leads to a mixture of products due to the insertion of oxygen into one or more P–C bonds. ^{31}P NMR spectroscopy in solution and in the solid state, as well as IR spectroscopy reveal distinct features of the phosphine oxides as compared to their H_2O_2 adducts. The single crystal X-ray analyses of $Bu_3P=O$ and $[Cy_3P=O \cdot (H_2O_2)]_2$ show a P=O stacking motif for the phosphine oxide and a cyclic structure, in which the six oxygen atoms exhibit a chair conformation for the dimeric H_2O_2 adduct. Different methods for the decomposition of the bound H_2O_2 and the removal of the ensuing strongly adsorbed H_2O are evaluated. Treating $R_3P=O \cdot (H_2O_2)_x$ with molecular sieves destroys the bound H_2O_2 safely under mild conditions (room temperature, toluene) within one hour and quantitatively removes the adsorbed H_2O from the hygroscopic phosphine oxides within four hours. At 60 °C the entire decomposition/drying process is complete within one hour.

Introduction

Phosphines represent one of the most important and ubiquitous classes of substances. Due to their unique properties they play prominent roles as ligands in coordination chemistry and catalysis.^{1,2} Phosphine oxides are equally important but receive less attention due to various factors. In some cases they are unavoidable stoichiometric side-products. This is, for example, the case for the Wittig reaction and its variations,³ the Staudinger reaction,⁴ or the Appel⁵ reaction. Separating the products from the phosphine oxides after these reactions can be rather tedious. In other cases, phosphine oxides might be the sign of insufficient exclusion of oxygen when the phosphine was the actual target molecule of any synthesis or application.

Every chemist working with phosphine ligands has to deal with phosphine oxides to some extent and these, in turn, can be oxidized to form a variety of products.⁶ Therefore, it is surprising that they do not receive more attention in the literature. Much of the knowledge about phosphine oxides within research groups working with phosphines is anecdotal. This is in part because they are elusive species regarding their nature and characterization. For example, they form adducts with H_2O ,⁷ boranes,⁸ or H_2O_2 .⁹ Furthermore, their ^{31}P NMR chemical shifts are very solvent

dependent (see below), and the chemical shift range is fairly uncharacteristic. Therefore, they can, for example, easily be confused with phosphonium salts.¹⁰ However, recently a systematic and mechanistic study has provided a deeper insight into the oxidation process of phosphines with molecular oxygen.^{6a} Phosphine oxides are also becoming increasingly important as probes for the surface acidity of oxide supports, such as silica or alumina, due to their strong interactions with surface hydroxyl groups. Most of these studies have been conducted using trialkyl phosphine oxides such as $Me_3P=O^{11a-e}$ and $Oct_3P=O^{11f}$ as the probes. Additionally, interesting metal complexes have been characterized with one,¹² two,¹³ or three¹⁴ oxygen-bound tertiary phosphine oxide ligands. Furthermore, there is a great potential in secondary phosphine oxides as pre-ligands in catalysis.¹⁵

The interest of our group in phosphine oxides is multi-fold. We need clean, adduct-free phosphine oxides with different electronic and steric characteristics for studying adsorption processes on oxide surfaces and the dynamics of the adsorbed species.¹⁶ Many of the strategically important phosphine oxides we require, such as $Sn(p-C_6H_4P(O)Ph_2)_4$,¹⁶ cannot be purchased and have to be synthesized from the corresponding phosphines. Furthermore, we have to be able to identify quickly and reliably the side-products that can form during the immobilization of phosphine linkers incorporating ethoxysilane groups on oxide surfaces.¹⁰ Therefore, baseline data regarding the NMR and IR spectroscopic characteristics of phosphine oxides and their adducts in solution and in the solid state is essential.

The main focus of this paper is threefold: (i) to explore quick and selective methods for the oxidation of phosphines, (ii) to systematically characterize phosphine oxides in solution and in

Department of Chemistry, Texas A&M University, P.O. Box 30012, College Station, TX 77842-3012. E-mail: bluemel@tamu.edu; Fax: (979)845-5629; Tel: (979)845-7749

† CCDC reference numbers 790886 and 845791 contain the crystallographic data for $Bu_3P=O$ (**2**) and $Cy_3P=O \cdot (H_2O_2)$ (**4a**), respectively. For crystallographic data in CIF or other electronic format see DOI: 10.1039/c1dt11863c

Table 1 ^{31}P NMR chemical shifts δ [ppm] of the phosphine oxides **1–5** and their corresponding hydrogen peroxide adducts **1a–5a** in C_6D_6 and CDCl_3 and the differences $\Delta\delta(^{31}\text{P}) = \delta(\text{adduct}) - \delta(\text{phosphine oxide})$

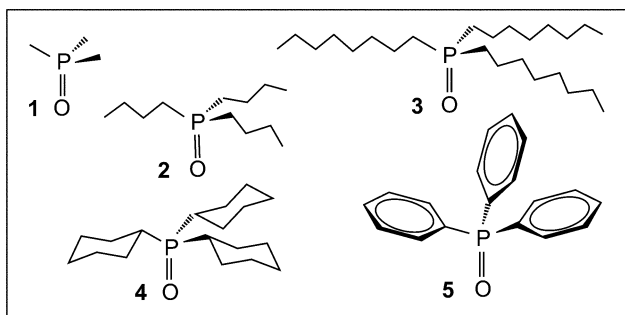
$\text{R}_3\text{P}=\text{O}/\text{H}_2\text{O}_2$ adducts	$\delta(^{31}\text{P})$ C_6D_6	$\Delta\delta(^{31}\text{P})$ C_6D_6	$\delta(^{31}\text{P})$ CDCl_3	$\Delta\delta(^{31}\text{P})$ CDCl_3
1/1a	32.65/ — ^a	— ^a	38.79/43.23	4.44
2/2a	43.66/51.12	7.46	48.57/52.50	3.93
3/3a	43.93/48.60	4.67	48.48/50.01	1.53
4/4a	46.31/50.28	3.97	49.91/51.53	1.62
5/5a	25.16/27.52	2.36	29.10/30.15	1.05

^a **1a** is not soluble enough in C_6D_6 to observe a signal.

the solid state by NMR and IR spectroscopy, as well as X-ray crystallography, and distinguish them from their H_2O_2 and H_2O adducts, and (iii) to explore methods that allow the safe, quick, and efficient purification of the phosphine oxides.

The most obvious method to obtain phosphine oxides is the exposure of the corresponding phosphines to air.^{6,17} However, this approach is surprisingly limited since many triaryl phosphines, such as triphenyl phosphine, even in solution are not efficiently oxidized in air. This phenomenon has recently been described mechanistically by Buchwald.^{6a} Another drawback is that the exposure of alkyl phosphines to air can afford numerous products involving insertions of oxygen into phosphorus-carbon bonds (see below).⁶ Methods to transfer one single oxygen atom per phosphine have been described,¹⁸ but the necessary reagents are not readily available and would have to be synthesized first.

Therefore, the alternative reaction with aqueous H_2O_2 will also be investigated here. Using a selection of representative alkyl and aryl phosphines, it will be demonstrated that the physical and spectroscopic characteristics of phosphine oxides and their water and hydrogen peroxide adducts are distinctly different from each other. Finally, methods to obtain the adduct-free representative alkyl and aryl phosphine oxides **1–5** (Scheme 1) are discussed. Two successful procedures are described, one of which is optimized.



Scheme 1 Representative tertiary phosphine oxides **1–5** used in this work.

Results and discussion

1. Distinguishing phosphine oxides from their H_2O_2 adducts

(a) NMR Spectroscopy. Probably the most intriguing part of working with phosphine oxides and their hydrogen peroxide adducts is that the chemical shifts are extremely solvent dependent. In order to obtain accurate chemical shift values with one measurement, we used ClPPh_2 as the chemical shift standard in a capillary insert centered in the NMR tubes (details: see

experimental section). Table 1 compares the ^{31}P chemical shifts of **1–5** and their corresponding H_2O_2 adducts **1a–5a** (generated as described below) in benzene and chloroform. For example, when **1** is measured in CDCl_3 instead of benzene the signal migrates downfield about 6 ppm. The dependence of $\delta(^{31}\text{P})$ on the solvent is less pronounced for the hydrogen peroxide adducts. Most probably, this reflects the fact that the $\text{P}=\text{O}$ group is strongly interacting with H_2O_2 by hydrogen bonding and is less prone to interactions with solvent molecules. However, even within this class of compounds, the ^{31}P NMR signal of **5a** migrates about 2.6 ppm downfield when changing the solvent from benzene to CDCl_3 . In general, benzene exerts a shielding effect on the $\text{P}=\text{O}$ group for both the phosphine oxides and their H_2O_2 adducts (Table 1).

Most significant analytically is the large change of the chemical shift when going from the phosphine oxides to their corresponding H_2O_2 adducts. Fig. 1 visualizes this dramatic effect for **2** and **2a** in C_6D_6 . As can be seen from the values given in Table 1, the chemical shift differences can amount to nearly 8 ppm (**2/2a**) in benzene. Overall, these shift differences between the substance classes are more pronounced in benzene than in CDCl_3 . As a general trend, the signals of the H_2O_2 adducts appear downfield from the phosphine oxides. This is in accordance with expectations since the hydrogen bonding of H_2O_2 to the oxygen of the $\text{P}=\text{O}$ group should lead to a deshielding of the phosphorus nucleus.

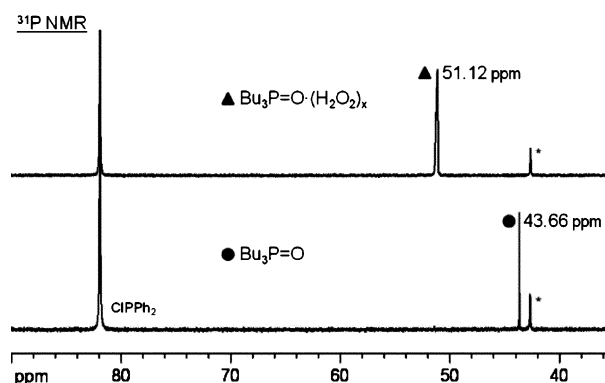


Fig. 1 ^{31}P NMR spectra of **2** (bottom trace) and **2a** (top trace) in C_6D_6 . The asterisks denote traces of $\text{Ph}_2\text{CIP}=\text{O}$ in the capillary, which stem from oxidation of the standard $\text{Ph}_2\text{P}=\text{O}$ (see experimental section).

In addition to the chemical shift issue, the lines of the H_2O_2 adducts are often broad due to the non-stoichiometric interactions of the phosphine oxides with H_2O_2 and H_2O , and exchanges with solvent molecules. Furthermore, larger aggregates might form due to the strong intermolecular hydrogen bonding with H_2O_2 .

Therefore, we investigated the dependence of $\delta(^{31}\text{P})$ of **2**, **2a**, **5**, and **5a** on their concentration in solution. Benzene has been chosen as the solvent for this quantitative analysis, because it leads to the largest $\delta(^{31}\text{P})$ difference between the phosphine oxides and their H_2O_2 adducts (Table 1). For **2** and **5**, the ^{31}P chemical shift changes with concentration are minimal. For example, $\delta(^{31}\text{P})$ of **5** varies within a 0.12 ppm range without a clearly distinguishable trend when increasing the concentration from 0.010 to 0.080 mol L⁻¹ (see experimental section for stepwise procedure). A concentration change from 0.10 to 0.75 mol L⁻¹ for **2** results in a chemical shift variation of 0.27 ppm. For both the H_2O_2 adducts **2a** and **5a**, the changes of $\delta(^{31}\text{P})$ are larger, and characteristic curves are obtained. Fig. 2 shows the graphical display for **2a**. Overall the chemical shift increases for **2a** (**5a**) by 0.87 (1.25) ppm when the concentration is changed from 0.10 (0.010) to 2.0 (0.080) mol L⁻¹. Since at very low concentrations the $\delta(^{31}\text{P})$ values for the adducts show a trend towards the phosphine oxides **2** and **5**, we conclude that the solvent is, to some extent, able to break up agglomerated molecules and replace the H_2O_2 . However, even with extreme dilution, the very different chemical shifts of the adduct-free phosphine oxides are not reached. Furthermore, the overall chemical shift changes over a dilution range of at least an order of magnitude are noticeable, but far from the $\delta(^{31}\text{P})$ differences between phosphine oxides and their corresponding H_2O_2 adducts.

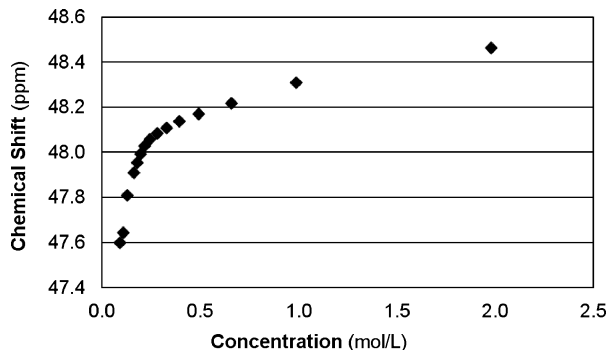


Fig. 2 Change of the $\delta(^{31}\text{P})$ of $\text{Bu}_3\text{P}=\text{O}\cdot(\text{H}_2\text{O}_2)$ (**2a**) with its concentration in C_6D_6 .

Since the phosphine oxides $\text{Me}_3\text{P}=\text{O}$ (**1**) and $\text{Bu}_3\text{P}=\text{O}$ (**2**) are hygroscopic (see below), the dependence of $\delta(^{31}\text{P})$ on the concentration of $2\cdot\text{H}_2\text{O}$ in C_6D_6 has also been investigated. The ^{31}P chemical shift of $\text{Bu}_3\text{P}=\text{O}\cdot\text{H}_2\text{O}$ changes from 44.35 to 43.60 ppm upon dilution of a 0.36 molar to a 0.05 molar solution, which results again in a noticeable but not crucial overall $\delta(^{31}\text{P})$ change of 0.75 ppm.

In contrast to **1** and **2**, the phosphine oxides **3–5** are not hygroscopic. $\text{Me}_3\text{P}=\text{O}$ (**1**) is even more hygroscopic than $\text{Bu}_3\text{P}=\text{O}$ (**2**),⁷ and any exposure to humid air changes the crystalline solid to an oil within less than 5 min. Fig. 3 illustrates the gravimetrically determined uptake of H_2O with time for **1** and **2**. $\text{Me}_3\text{P}=\text{O}$ not only absorbs H_2O faster but also a larger amount of it, as compared to **2**. Saturation is reached when the ratio of **1** : H_2O is about 1 : 3.5. On the same timeline, **2** is saturated when the ratio of **2** : H_2O is about 1 : 1.

In the previous section we described that with careful chemical shift referencing, it is possible to distinguish the phosphine oxides from their H_2O_2 adducts by ^{31}P NMR in solution. In the solid-

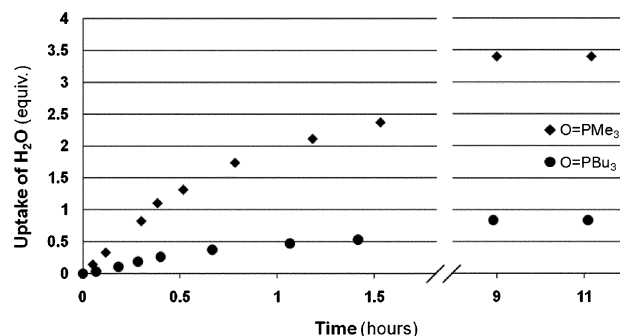


Fig. 3 Water uptake of $\text{Me}_3\text{P}=\text{O}$ (**1**) and $\text{Bu}_3\text{P}=\text{O}$ (**2**) in air.

state NMR spectra,¹⁹ due to the lack of solvent interactions and exchange equilibria, narrow lines are expected for the polycrystalline materials. Unfortunately, most of the phosphine oxides **1–5** and especially the H_2O_2 adducts **1a–5a** are liquids or low-melting solids (see Fig. 11 below) that would undergo a phase change under the pressures and elevated temperatures²⁰ of MAS (Magic Angle Spinning).¹⁹ But for the pairs **4/4a** and **5/5a**, the CSA (chemical shift anisotropy)^{19a} data and ^{31}P MAS spectra could be obtained. Fig. 4 and 5 show, for example, the MAS and wide-line spectra of **5** and **5a**. In accordance with our expectation for crystalline material, the residual linewidths of the isotropic peaks in the MAS spectra are only 166 Hz for **5** and 261/268 Hz for the two lines of **5a**. The isotropic lines can easily be determined by varying the rotational speed because in contrast to the rotational sidebands, they are static and do not change their positions.

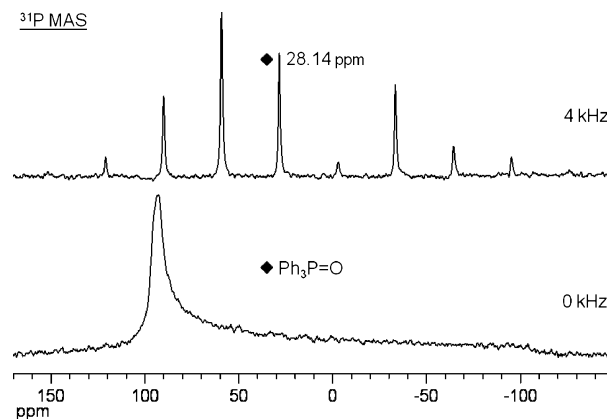


Fig. 4 ^{31}P MAS (top, 4 kHz) and wide-line (bottom, 0 kHz) spectra of polycrystalline **5**. The $\delta(^{31}\text{P})$ value is given for the isotropic chemical shift in the MAS spectrum; the other lines are rotational sidebands.

The $\delta(^{31}\text{P})$ of 28.14 ppm for the isotropic line in the solid-state NMR spectrum of **5** (Fig. 4) lies within the chemical shift ranges found in solution (Table 1). There is only one isotropic line for **5**, as expected from earlier results²¹ and tri(*p*-tolyl)phosphine oxide.^{21c} This is also in accordance with the single crystal X-ray structures of **5**²² or **2** (see below), which imply that all phosphorus nuclei in the unit cell are magnetically equivalent.

In contrast, the polycrystalline H_2O_2 adduct **5a** displays two isotropic lines in the ^{31}P MAS spectrum (Fig. 5). The chemical shifts of 31.01 and 27.90 ppm are close to the values found in solution (Table 1). Since the intensity ratio of both lines, including the rotational sideband intensities in the integration, is about 1 : 1,

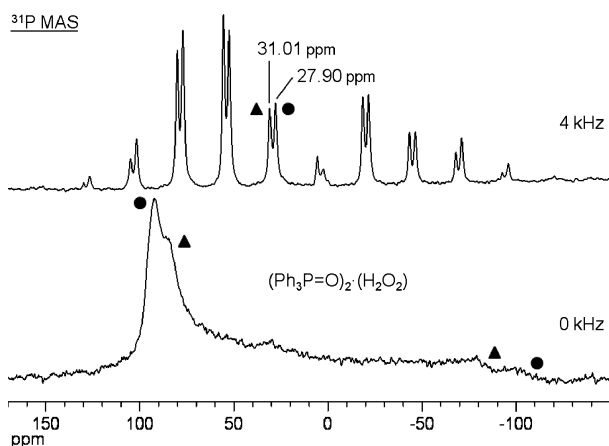


Fig. 5 ^{31}P MAS (top, 4 kHz) and wideline (bottom, 0 kHz) spectra of polycrystalline **5a**. The $\delta(^{31}\text{P})$ values are given for the two isotropic chemical shifts in the MAS spectrum; the other lines are the rotational sidebands. The symbols represent the δ_{11} and δ_{33} of the two corresponding CSA patterns.

the presence of polymorphs is unlikely. The two isotropic lines most probably stem from two magnetically inequivalent phosphorus nuclei in the unit cell. This is corroborated by the single crystal X-ray structure of the compound $(\text{Ph}_3\text{P}=\text{O})_2 \cdot (\text{H}_2\text{O}_2)$,^{9c} where one H_2O_2 molecule bridges two $\text{Ph}_3\text{P}=\text{O}$ molecules, which leads to two magnetically independent phosphorus nuclei in the unit cell. Additionally, the unit cell of the single crystal of $\text{C}_y\text{P}=\text{O} \cdot (\text{H}_2\text{O}_2)$ (see below) contains two magnetically inequivalent P nuclei. The splitting of isotropic lines in the ^{31}P MAS spectra of polycrystalline compounds is also often observed for chelate phosphine ligands and metal complexes thereof. For example, $(\text{Ph}_2\text{PCH}_2)_3\text{SiOEt}$ featured three isotropic lines with equal intensities but with a large difference in their chemical shifts.²³ $(\text{Ph}_2\text{PCH}_2)_2\text{Si}(\text{OEt})_2$ and diverse nickel complexes with chelate phosphine ligands^{19d,23} always gave two isotropic lines with similar chemical shifts.

$\text{Cy}_3\text{P}=\text{O}$ (**4**) and its H_2O_2 adduct **4a** exhibit analogous solid-state NMR characteristics. The only isotropic signal of **4** has a chemical shift of 47.28 ppm, which lies within the δ ranges found in solution. The residual linewidth is only 158 Hz, so overlapping of two or more isotropic signals is unlikely. Analogous to **5a**, the ^{31}P MAS spectrum of the polycrystalline H_2O_2 adduct **4a** displays two isotropic lines with a 1 : 1 intensity ratio of the signals including the rotational sidebands. The chemical shifts of 51.53 and 53.61 ppm are again close to the values found in solution (Table 1).

The ^{31}P MAS spectra of the triarylphosphine oxide **5** and its H_2O_2 adduct **5a** could be obtained with only 64 scans at the moderate spinning speeds of 4 and 5 kHz. Therefore, the wideline spectra without rotation could be recorded as well (Fig. 4 and 5). The chemical shift anisotropy of **5**, defined as the span of the wideline signal,^{19a} is about 200 ppm and therewith matches the literature values for **5** (CSA 195–200 ppm),²¹ for tri(*p*-tolyl)phosphine oxide (CSA 155 ppm),^{21c} or for the trialkylphosphine oxide ($n\text{-C}_{14}\text{H}_{29}$)₃ $\text{P}=\text{O}$ (CSA 190 ppm).^{21a} The CSA of the ^{31}P wideline signal of **5a** is substantially smaller with about 170 and 200 ppm for the two ^{31}P wideline signals (Fig. 5).

The reduction of the CSA on going from a phosphine oxide to its adduct is even more pronounced for the pair **4/4a**. The span of the wideline signal is about 153 ppm for **4** and about 128 and

147 ppm for **4a**. In this case, however, the wideline patterns of both signals are not as clearly distinct as for **5a**.

The general CSA reduction on going from the phosphine oxides to their H_2O_2 adducts reflects the fact that with the adduct formation the $\text{P}=\text{O}$ bond order and its polarity decrease, in accordance with the IR analysis (see below). For example, in the extreme case of decreasing the $\text{P}=\text{O}$ bond order on going from $\text{Ph}_3\text{P}=\text{O}$ to $[\text{Ph}_3\text{POEt}]\text{BF}_4$ the CSA decreases from 195–200 ppm^{21a,b} to 74 ppm.^{10c} In analogy to H_2O_2 adduct formation, substantial reduction in the CSA is also observed when phosphine oxides are adsorbed on oxide supports, such as silica, as the $\text{P}=\text{O}$ groups interact with surface silanol groups and undergo partial quaternization.¹⁶

(b) Crystallography. The crystal structure of a water clathrate of **2** ($2 \cdot (\text{H}_2\text{O})_{34.5}$) has been reported,²⁴ but not the pure substance. Accordingly, suitable crystals of **2** were obtained, X-ray data were collected, and the structure was solved as described in the experimental section. This gave the structures displayed in Fig. 6 and 7.

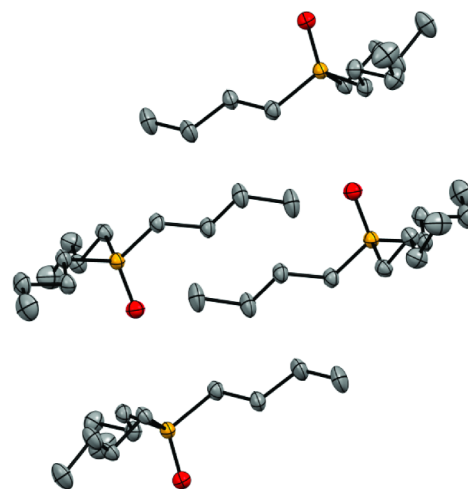


Fig. 6 Single crystal X-ray structure of $\text{Bu}_3\text{P}=\text{O}$ (**2**), view showing the aligned $\text{P}=\text{O}$ bonds. Selected bond lengths (\AA) and angles ($^\circ$): P(1)–O(1) 1.489(2), P(1)–C(1) 1.797(3), P(1)–C(5) 1.798(2), P(1)–C(9) 1.798(2), O(1)–P(1)–C(1) 113.10(10), O(1)–P(1)–C(5) 112.90(10), O(1)–P(1)–C(9) 113.11(10).

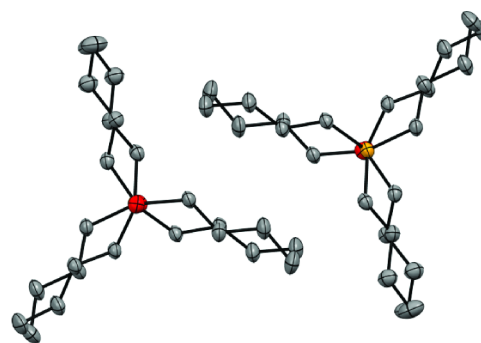


Fig. 7 Single crystal X-ray structure of $\text{Bu}_3\text{P}=\text{O}$ (**2**), view along the $\text{P}=\text{O}$ bond.

The bond lengths and angles about phosphorus (Fig. 6) were routine. Presumably due to dipole–dipole interactions, a

O=P...O=P stacking motif was observed. This has also been found with other crystalline phosphine oxides such as **4**²⁵ and **5**.²² These stacking motifs may be relevant for the potential formation of bilayers on silica surfaces.¹⁶ The intermolecular O...P distance, 3.587 Å, exceeds the sum of the van der Waals radii of the oxygen and phosphorus atoms (1.52 and 1.80 Å).²⁶ The adjacent P=O linkages within a stack are not perfectly aligned, as reflected by intermolecular O-P-O and P-O-P angles of 179.2° and 174.0°.

The butyl groups crystallize in all-anti conformations. Fig. 7 illustrates that the butyl groups are slightly staggered between adjacent molecules in a stack, as quantified by a C1-P-P-C1 torsion angle of 38.8°. Importantly, the structure does not contradict the finding of only one isotropic line in the MAS spectra of **4** and **5** (see above).

Only one crystal structure of a H₂O₂ adduct of a phosphine oxide, the 2:1 complex **5**·HOOH·**5** or (Ph₃P=O)₂·(H₂O₂), has been previously reported.^{9c} Suitable crystals of the 1:1 complex **4a** were obtained as described in the experimental section. X-ray data were collected and the structure was solved in a routine manner that included the location and refinement of the oxygen-bound hydrogen atoms. This gave the cyclic dimeric structure (C₃P=O·H₂O₂)₂ or (**4a**)₂ displayed in Fig. 8 and 9. The adduct features two hydrogen bonds to each phosphine oxide oxygen atom, with an inversion center in the midpoint of the plane formed by the four H₂O₂ oxygen atoms.

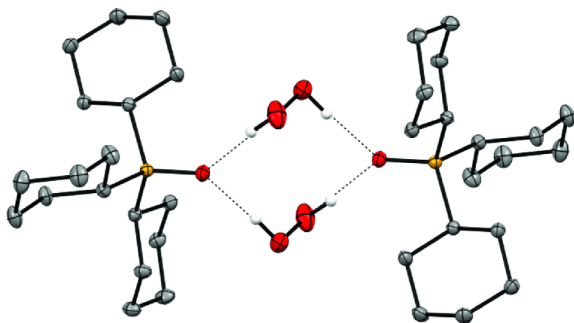


Fig. 8 Single crystal X-ray structure of the dimer of **4a**. Selected bond lengths (Å) and angles (°): P(1)–O(1) 1.5045(9), P(1)–C(1) 1.8190(12), P(1)–C(7) 1.8209(12), P(1)–C(13) 1.8258(12), O(1)–P(1)–C(1) 111.03(5), O(1)–H(20) 1.876, H(20)–O(20) 0.896, O(20)–O(21) 1.4504(15), O(21)–H(21) 0.895, O(1)–P(1)–C(1) 113.03(5), O(1)–P(1)–C(7) 109.92(5), O(1)–P(1)–C(13) 112.04(5), P(1)–O(1)–H(20) 129.1, O(1)–H(20)–O(20) 176.0, (H20)–O(20)–O(21) 103.2, (O20)–O(21)–H(21) 100.4.

The P=O linkage in (**4a**)₂ proves to be somewhat longer than that in the corresponding phosphine oxide **4**²⁵ (1.5045(9) vs. 1.490(2) Å). The P=O...H distance (1.876 Å) is in the typical range for hydrogen bonds, and the O...O distance in the P=O...H–O unit (2.743 Å) compares with that in (Ph₃P=O)₂·(H₂O₂) (2.759 Å), for which the oxygen-bound hydrogen atom could not be located.^{9c}

The cyclohexyl rings and the assembly defined by the six oxygen atoms adopt chair conformations. In the latter, the HO–OH distance is within experimental error of that in crystalline H₂O₂ (1.4504(15) vs. 1.453(7) Å).²⁷ The dihedral angles defined by the HO–OH and (P=O)...O–O...(O=P) units (89.54° and 87.10°) are also very close to the dihedral angle in crystalline H₂O₂

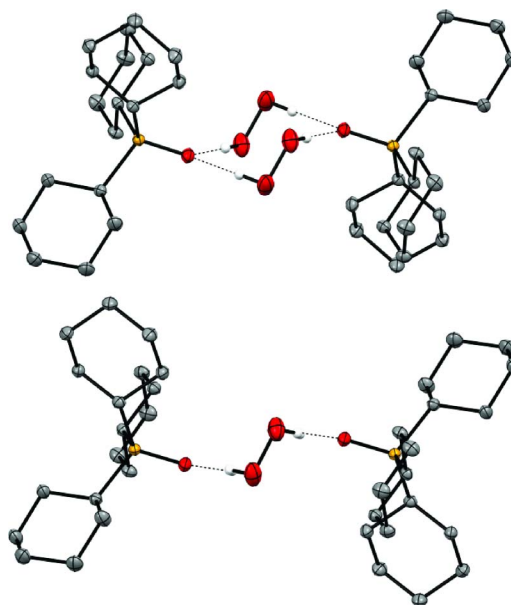


Fig. 9 Additional views of the single crystal X-ray structure of the dimer of **4a**. Top: tilted side view, bottom: side view.

(90.2(6)°). Hence, the structure of H₂O₂ is not appreciably affected by bonding to **4**.

Importantly, Fig. 8 and 9 corroborate the finding of two isotropic lines in the ³¹P solid-state NMR spectra of the H₂O₂ adducts of the phosphine oxides, because there are two magnetically independent phosphorus nuclei in the unit cell.

(c) IR Spectroscopy. IR spectroscopy²⁸ provides unique insight into the phosphine oxide and H₂O₂ adduct scenario because it probes both the P=O groups^{9b,29} and all O–H species^{9b} via their stretching vibrations. As in solid-state NMR, the IR spectra can be recorded using the neat liquid or polycrystalline samples, and therefore, the results are independent of any interactions of the functional groups with solvents. Fig. 10 shows, as a representative case, the IR spectra of **2** (top), **2a** (bottom), and **2a** after partial decomposition of the bound H₂O₂ as described below (middle). Table 2 summarizes key IR data.

As the predominant analytical features, the spectrum of **2** (Fig. 10, bottom) shows only the bands typical for C–H stretching absorptions below 3000 cm⁻¹ and the P=O stretching band at 1153 cm⁻¹. All bands are very narrow, indicating that the vibrations within the molecules are well-defined.

In contrast, while the C–H stretching bands are practically unchanged as compared to **2**, the IR spectrum of **2a** (Fig. 10, top) shows a broad O–H stretching band for the bound H₂O₂

Table 2 IR absorptions [ν] of the phosphine oxides **1–5** and their corresponding H₂O₂ adducts **1a–5a** and the wavenumber differences $\Delta\nu(\text{P=O}) = \nu(\text{phosphine oxide}) - \nu(\text{adduct})$

R ₃ P=O/H ₂ O ₂ adduct	$\nu(\text{P=O})/\text{cm}^{-1}$	$\Delta\nu(\text{P=O})/\text{cm}^{-1}$	$\nu(\text{O–H})$ of 1a–5a /cm ⁻¹
1/1a	1161/1094	67	3217
2/2a	1153/1123	30	3217
3/3a	1144/1142	2	3217
4/4a	1157/1138	19	3264
5/5a	1188/1174	14	3233

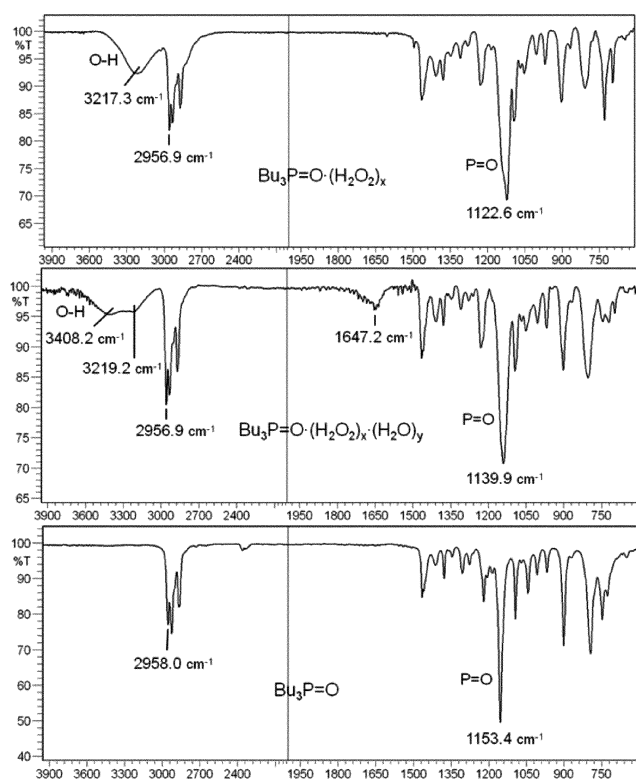


Fig. 10 IR spectra of neat **2** (bottom), **2a** (top), and **2a** with adsorbed H_2O after partial decomposition of the bound H_2O_2 (middle).

at 3217 cm^{-1} .^{9b} The intense $\text{P}=\text{O}$ band has shifted to the lower wavenumber of 1123 cm^{-1} . This indicates that the $\text{P}=\text{O}$ bond order has decreased, rendering the corresponding stretching vibration lower in energy. This change goes along with the broadening of the line because of the less well-defined vibrations due to the hydrogen bonding interactions with the H_2O_2 molecules.

When the H_2O_2 molecule in **2a** is partially decomposed thermally, the H_2O strongly binds to the $\text{P}=\text{O}$ group. Its O–H stretching vibration is distinctly different from that of bound H_2O_2 , but its band at 3408 cm^{-1} is also broad, as can be seen in the middle spectrum of Fig. 10. The stretching band of the residual H_2O_2 molecules remains practically unchanged at 3219 cm^{-1} . As an additional, analytically useful feature, the overtone of the O–H absorption of the H_2O band appears at about 1647 cm^{-1} , as described in the literature for adducts of $\text{Ph}_3\text{P}=\text{O}$.^{9b} Again, the $\text{P}=\text{O}$ stretching frequency is broad and found at a lower wavenumber (1140 cm^{-1}) for $2\cdot(\text{H}_2\text{O}_2)_x(\text{H}_2\text{O})_y$ ($x, y = 0.5\text{--}1.0$) than for **2**.

Overall, IR spectroscopy is a powerful tool for quickly analyzing the nature and purity of phosphine oxides and their various adducts, and it was primarily used in the following experiments for characterizing all involved species and optimizing the two most promising procedures for obtaining clean phosphine oxides.

2. Controlled decomposition of the hydrogen peroxide adducts **1a–3a** to give the phosphine oxides **1–5**

(a) Syntheses of **1a–5a.** When phosphines are oxidized in air, especially trialkyl phosphines, a multitude of byproducts are possible besides the desired phosphine oxides $\text{R}_3\text{P}=\text{O}$. Only Me_3P gives $\text{Me}_3\text{P}=\text{O}$ (**1**) in a reasonably clean reaction, most probably

due to the fast oxidation process. The same is true for neat Ph_2PH , which forms $\text{Ph}_2\text{HP}=\text{O}$ exclusively in a radical oxidation process when exposed to air.¹⁷ The predominant side-reaction is the additional insertion of oxygen atoms into P–C bonds⁶ to form mainly phosphinic and phosphonic and occasionally phosphoric acid esters that can be identified by their $\delta(^{31}\text{P})$.^{6,10a,19e} For example, when toluene solutions of Bu_3P are exposed to air, a typical ^{31}P NMR spectrum would show the signal of the desired product $\text{Bu}_3\text{P}=\text{O}$ (**2**, 43.34 ppm, 44%), as well as resonances for the phosphinic acid ester $\text{Bu}_2(\text{BuO})\text{P}=\text{O}$ (53.96 ppm, 45%), the phosphonic acid ester $\text{Bu}(\text{BuO})_2\text{P}=\text{O}$ (36.28 ppm, 7%), traces of unidentified oxidation products (around 30 ppm) and unreacted phosphine (-32.20 ppm). The product ratio does not change with the reaction time, and we could not optimize this reaction to give only, or at least predominantly, **2**. Even if it was feasible to separate the product from the reaction mixture, all the side-products still lead to a diminished yield of phosphine oxide.

As an additional complicating factor, H_2O from the humid air can be adsorbed due to the formation of hydrogen bonds with the $\text{P}=\text{O}$ group, rendering the analysis of mixtures by ^{31}P NMR difficult (see above). This H_2O uptake takes place preferentially with short alkyl chain substituents R , as discussed above. Triarylphosphines might not be oxidized by air at all.^{6a} For example, Ph_3P is not transformed into the oxide **5** when dissolved in a nonpolar solvent and exposed to the ambient atmosphere for months. Taking all these limitations into account, the oxidation of phosphines by simple exposure to air is not a feasible or efficient way to obtain clean tertiary phosphine oxides. This overall scenario might also be responsible for the frustration that researchers can experience when handling phosphines without carefully excluding air.

In contrast, when H_2O_2 is employed as the oxidant in the synthesis of phosphine oxides, no byproducts are obtained, and the reaction proceeds smoothly at room temperature and in a well-defined manner. However, H_2O_2 molecules form hydrogen bonds to the oxygen of the $\text{P}=\text{O}$ group and adducts of the type $\text{R}_3\text{P}=\text{O}\cdot(\text{H}_2\text{O}_2)_x$ with $x = 0.5$ to 1.0 are obtained. Interestingly, although the oxidation with hydrogen peroxide is performed in the presence of water, the latter seems to form weaker adducts and is not competitive, so that only H_2O_2 is bound to the products (Fig. 10, top spectrum). The single crystal X-ray analysis of **5a** proves that two molecules of **5** are bound to one bridging H_2O_2 molecule.^{9c} On the other hand, in the case of a H_2O_2 adduct of $\text{Ph}_3\text{As}=\text{O}$, a hydrogen-bonded network with a 1 : 1 ratio of arsine oxide to H_2O_2 has been found.³⁰ The hydrogen peroxide adducts **1a–3a** most likely have a less well-defined H_2O_2 to $\text{R}_3\text{P}=\text{O}$ ratio as they have an oily appearance and thus can easily be distinguished from the phosphine oxides **1–3**, which are all colorless powders. This is displayed for **2** and **2a** in Fig. 11.

(b) Possible methods for decomposing the hydrogen peroxide adducts **1a–5a to give the phosphine oxides **1–5**.**

There are several known approaches for decomposing H_2O_2 attached to phosphine oxides by hydrogen bonds. Bimetallic Pt–Pd surfaces are, for example, known to decompose H_2O_2 .³¹ Additionally, copper^{9a} is reported to achieve the decomposition and also MnO_2 .^{9a} Furthermore, the adducts can be heated ($> 100\text{ }^\circ\text{C}$) to release the oxygen from the bound H_2O_2 .^{9a} However, with the latter method, care has to be taken since the oxygen release can happen

Table 3 Melting points and decomposition temperature ranges [°C] of the phosphine oxides **1–5** and their corresponding H₂O₂ adducts **1a–5a**

R ₃ P=O/H ₂ O ₂ adduct	Decomp. temp. of neat H ₂ O ₂ adduct ^a	m.p. of neat R ₃ P=O, obs.	m.p. of neat R ₃ P=O ^{ref.}
1/1a	63–94	135–139	137.5–138.5 ³³
2/2a	98–149	59–63	63–64 ³⁴
3/3a	88–140	48–52	48–50 ³⁵
4/4a	120–134	158–160	155–157 ¹²
5/5a	136–183	155–157	156.5–158 ³⁶

^a Values based on the appearance of small bubbles in the capillary during heating, which are attributed to evolution of oxygen from H₂O₂ decomposition.

**Fig. 11** Physical appearance of neat Bu₃P=O (**2**, right) and Bu₃P=O·(H₂O₂)_x (**2a**, left, *x* = 0.5–1.0) in a vial.

quickly, resulting in violent explosions. We tested and evaluated a selection of the known procedures for the decomposition of H₂O₂ attached to phosphine oxides and optimized new methods that also efficiently remove the resulting H₂O quantitatively.

Surprisingly, when we treated **2a** in benzene with freshly cut pieces of a Cu wire, even at higher temperatures and after prolonged exposure, no H₂O₂ decomposition occurred as assayed by IR spectroscopy. However, when **2a** was treated with MnO₂ powder, O₂ evolved immediately and vigorously, and IR spectroscopy confirmed the complete decomposition of H₂O₂. Unfortunately, the H₂O formed during this process remains strongly bound to **2a**. Furthermore, the fine MnO₂ powder could not be removed by standard filtration processes, rendering this process impractical.

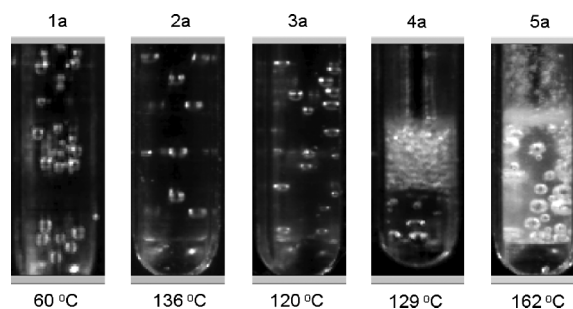
Next, we tried silica as a model material for glass with a high surface area because it is generally known that aqueous H₂O₂ decomposes with time at the walls of glass bottles.^{9a} Indeed, when stirring **2a** in toluene overnight with a slurry of silica that had not been dried prior to its application (“wet” silica, containing adsorbed H₂O and a maximal number of surface OH groups),³² H₂O₂ decomposition was complete. However, IR revealed that the formed H₂O was still attached to **2a**, and it could not be removed by treating the material with Na₂SO₄ or MgSO₄.

Since we had so far not found a way to obtain the water-free phosphine oxides from the hydrogen peroxide adducts, we investigated the option of thermal decomposition because then we would at least avoid further product separation steps. Heating **2a** in a toluene solution in order to decompose the attached H₂O₂ to obtain **2a**·(H₂O)_x required 36 h and temperatures of up to 95 °C. Besides still being confronted with the task to remove the bound water, another practical drawback of this method is the time consuming removal of the relatively high-boiling solvents required. Therefore, we studied the decomposition of the neat adducts **1a–5a**. We worked on a small scale in melting point tubes

behind safety glass because according to our experience, H₂O₂ adducts of phosphines can lead to explosions when heated in neat form.

Table 3 summarizes the data obtained from the neat materials and provides the literature values for comparison. The decomposition of the bound H₂O₂ happens well below the actual boiling point of the corresponding adduct-free phosphine oxide.

As illustrated in Fig. 12, the effervescence indicates the release of O₂ gas as H₂O₂ is broken down. The onset of the decomposition, as well as its temperature range, varies greatly between the adducts (Table 3). Naturally, the decomposition process is better visible for the viscous liquids **1a–3a** than for the powders **4a** and **5a**. Interestingly, for both **2a** and **3a** we found that at around 150 °C there is a sudden onset of the formation of larger bubbles. We assign this phenomenon to the release of bound H₂O because this temperature is still well below the boiling points of **2a** and **3a**.

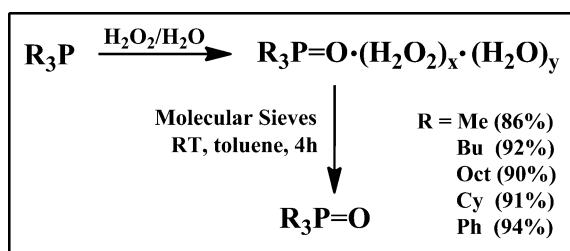
**Fig. 12** Evolution of small O₂ bubbles during decomposition of the neat materials R₃P=O·(H₂O₂)_x (*x* = 0.5–1.0) at the given temperatures (**1a–5a**).

While the decomposition of the bound H₂O₂ in neat **1a–5a** is clearly possible, this method suffers from the fact that water still remains in the samples. Furthermore, high temperatures are needed, and scaling up this process poses a safety risk. Therefore, as described in the following paragraph, we optimized two new methods that can be applied safely in any laboratory and leads to the clean phosphine oxides in a straightforward manner.

(c) Optimized method for decomposing the hydrogen peroxide adducts 1a–5a to give the phosphine oxides 1–5. All methods described in the previous section lead to the water adducts of the phosphine oxides and not the clean species R₃P=O. One of the safest methods consists of the treatment with silica, which can easily be separated from the supernatant with the product after the reaction. Therefore, instead of using the “wet” silica, we performed the same reaction with silica pre-dried at 200 °C for seven days *in vacuo*. The resulting silica surface should consist largely of siloxane groups with only a minimal number of residual silanol moieties,³² which might have the potential to compete with the phosphine

oxides for the formed H_2O by adsorbing it. Being less reactive, pre-dried silica is our preferred support material for immobilized catalysts.^{2,37} The diminished reactivity of a slurry of pre-dried silica in toluene manifests itself in the prolonged time of about 4 d needed to decompose the H_2O_2 in **2a**. Fortunately, however, IR spectroscopy of the supernatant proves the disappearance of O–H stretching bands for both H_2O_2 and residual water. The adduct-free and clean phosphine oxides can be obtained in this way. The only drawback of using silica is that phosphine oxides are strongly adsorbed at its surface.¹⁶ Therefore, in order to diminish the loss of product, several wash cycles are required to detach the phosphine oxides from the silica surface.

Our quest for a material that would decompose the H_2O_2 in **1a–5a** and at the same time quickly remove the resulting H_2O while releasing the phosphine oxides **1–5** easily after the reaction, led us to molecular sieves. This material seemed promising to us because it is known to decompose 30% aqueous H_2O_2 at 80 °C.³⁸ Indeed, pre-dried molecular sieves with 3 Å pore diameter allowed us to obtain the clean phosphine oxides from the corresponding phosphines in very high yields of up to 94% (Scheme 2). Most of the loss in the yield occurs in the biphasic oxidation step, as this requires the separation of organic and aqueous layers, and some of the H_2O_2 adducts of the phosphine oxides are rather soluble in water. The loss of the phosphine oxide products due to adsorption has been determined by model reactions to be minimal, less than 2 mol% per g of molecular sieves with the amounts and ratios of solids to phosphine oxides given in the experimental section. The reason for this is that, in contrast to silica,³² molecular sieves do not have a large number of acidic protons on the surface, which could strongly interact with the free electron pairs of phosphine oxides.



Scheme 2 Yields of clean phosphine oxides **1–5** with respect to the corresponding phosphines after oxidation with hydrogen peroxide to form **1a–5a**, decomposition of attached H_2O_2 , and removal of water with molecular sieves ($x, y = 0.5–1.0$).

Using the molecular sieves, both the decomposition of H_2O_2 and the removal of H_2O from the hygroscopic phosphine oxides were complete within 4 h at room temperature. At the elevated temperature of 60 °C the whole process is complete within 1 h. The molecular sieves are best placed into a tea bag in order to facilitate stirring and their retrieval after the reaction (Fig. 13). This protocol is safe and can easily be scaled up, and amounts of more than 5 g of molecular sieves pose no problem.

Conclusions

It has been demonstrated that the ^{31}P NMR chemical shifts of phosphine oxides and their hydrogen peroxide and water adducts are very different. Furthermore, the ^{31}P solid-state NMR charac-

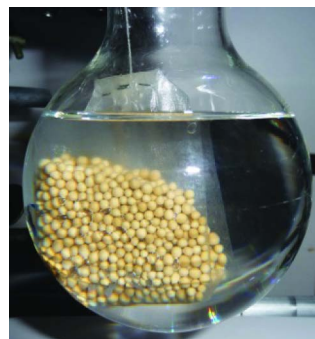


Fig. 13 Molecular sieves placed in a tea bag and suspended in toluene in a round bottom flask for easy removal after the reaction.

teristics of the clean phosphine oxides are distinctly different from those of the hydrogen peroxide adducts. IR spectroscopy has been applied to distinguish between the neat phosphine oxides, their hydrogen peroxide adducts, and to detect adsorbed water. Single crystal X-ray structures of $\text{Bu}_3\text{P}=\text{O}$ and $\text{Cy}_3\text{P}=\text{O}\cdot(\text{H}_2\text{O}_2)$ have been determined, the latter being the first of its type. With IR spectroscopy, a method using molecular sieves could be optimized for the safe and quick decomposition of the bound hydrogen peroxide. The molecular sieves also efficiently and quantitatively remove the water formed in this process. The yields of the clean phosphine oxides are nearly quantitative since phosphine oxides are only weakly adsorbed at the surface of the molecular sieves.

Experimental

(a) General procedures

All reactions involving phosphine starting materials were performed under a purified nitrogen atmosphere. Phosphine oxides were stored under nitrogen. Chemicals were treated as follows: toluene (Mallinckrodt Chemicals, ACS grade) was distilled from Na/benzophenone and CH_2Cl_2 (Mallinckrodt Chemicals, HPLC grade) was dried in a commercially available MBraun solvent purification system. C_6D_6 (Cambridge Isotope Laboratories) and CDCl_3 (Aldrich) were dried over 3 Å molecular sieves (EMD Chemical Inc.). The latter was also used for obtaining the adduct-free phosphine oxides, and it has the approximate composition (weight percentages): silica gel < 50%, Al_2O_3 < 40%, Na_2O < 30%, K_2O < 15%, MgO < 5%, and quartz < 3%. The molecular sieves were activated by heating in vacuum at 120 °C for 12 h. Bu_3P (Strem Chemicals, 99%), Oct_3P (Alfa Aesar, 90% technical), and Cy_3P (Alfa Aesar) were purified by column chromatography (alumina, elution with CH_2Cl_2). Me_3P (Alfa Aesar, 99%) and CIPPh_2 (TCI America, 98%) were used as received but kept in a glove box. H_2O_2 (Acros Organics, 35% aqueous solution) was either used as obtained or diluted and stored at 4 °C. Ph_3P (Aldrich, 99%), MnO_2 (Alfa Aesar, technical, min. 58%), and silica (Merck, 40 Å average pore diameter, 0.063 to 0.2 mm average particle size, specific surface area 750 $\text{m}^2 \text{g}^{-1}$) were used as obtained. In addition to the latter “wet” silica, a “dry” batch was generated by heating the silica for 7 d at 200 °C at the vacuum line.

The ^1H , $^{13}\text{C}\{^1\text{H}\}$, and $^{31}\text{P}\{^1\text{H}\}$ NMR spectra of liquids were recorded on a 500 MHz Varian spectrometer at 499.70, 125.66, and 470.17 MHz. The ^1H and ^{13}C chemical shifts were referenced using the solvent signals. For ^1H NMR, the residual protons in

the deuterated solvents (C_6D_5H , 7.15 ppm; $CHCl_3$, 7.26 ppm) were used; for ^{13}C NMR the carbon signals (C_6D_6 , 128.02 ppm; $CDCl_3$, 77.00 ppm). For the accuracy of the ^{31}P NMR chemical shifts of solutions, $CIPPh_2$ (neat liquid, $\delta(^{31}P) = 81.92$ ppm) was used as a chemical shift standard within a capillary centered in the 5 mm sample tubes. The signal assignments were based on previous results^{2a,39} and confirmed by 2-dimensional $^1H, ^1H$ COSY and $^1H, ^{13}C$ COSY NMR correlation spectroscopy experiments. Since the literature data are fragmentary, all 1H , ^{13}C , and ^{31}P NMR data obtained in two different solvents (C_6D_6 and $CDCl_3$) are given below.

The ^{31}P solid-state NMR spectra were recorded on a 400 MHz Bruker Avance widebore NMR spectrometer equipped with a 4 mm broadband probehead and ZrO_2 rotors. The polycrystalline substances were densely packed into the rotors. The chemical shifts were referenced with polycrystalline $(NH_4)H_2PO_4$ (+0.81 ppm) as the external standard. A single pulse program with 1H high-power decoupling was applied, and typically about 3000 scans with a pulse delay of 10 s were sufficient to obtain a good signal-to-noise ratio.

IR data of the neat powders and viscous liquids were recorded on a Shimadzu IRAffinity-1 FTIR instrument using a Pike Technologies MIRacle ATR plate. Melting point videos were obtained in open capillaries with a Stanford Research Instruments MPA100 OptiMelt system.

(b) Synthesis and purification of phosphine oxides

Representative procedure for the synthesis of the H_2O_2 adducts of the phosphine oxides (1a–5a). For each oxidation the same procedure was applied, except for minor deviations for **1a** and **5a**, which are described below. Representative procedure: Bu_3P (3.552 g, 17.56 mmol) was dissolved in 150 mL of toluene in a Schlenk flask, which was cooled to 0 °C. Then ten equivalents of concentrated aqueous H_2O_2 solution (35 weight % in H_2O , 17.10 mL, 176.0 mmol H_2O_2) were added dropwise *via* syringe with vigorous stirring. The reaction mixture was stirred overnight and allowed to slowly warm to room temperature. After 12 h, the toluene layer was transferred into a round bottom flask with a metal cannula. ^{31}P NMR proved that the oxidation process is quantitative. The aqueous layer was washed with toluene (3 × 20 mL), and all organic phases were combined. The solvent was removed *in vacuo*, and **2a** was obtained as a colorless viscous liquid (3.751 g, 84.7% yield, assuming one H_2O_2 molecule per one phosphine oxide molecules). All H_2O_2 phosphine oxide adducts **1a–5a** were characterized by ^{31}P NMR and IR spectroscopy, as well as their melting points (see Tables 1–3 above). The hydrogen peroxide adducts **1a–3a** were colorless oils while **4a** and **5a** were white crystalline solids.

The H_2O_2 adduct **1a** was highly water soluble, so it could not be efficiently extracted into toluene or other polar organic solvents, such as diethyl ether, THF, CH_2Cl_2 , and ethyl acetate. Therefore, after the oxidation step, all volatile matter (solvents, excess H_2O_2 , H_2O) was removed *in vacuo* at 40 °C. Excess water remained hydrogen-bonded to the adduct **1a** (see results and discussion section).

For **5a**, no more than ~2 g of **5** per 150 mL of toluene should be used for the oxidation step because **5a** showed a tendency to precipitate due to its low solubility in toluene. Alternatively, **5a**

was be extracted from the aqueous layer with CH_2Cl_2 , or the entire synthesis performed using CH_2Cl_2 instead of toluene as the solvent.

Representative procedure for measuring $\delta(^{31}P)$ depending on the concentration of **2, **2a**, **5**, and **5a**.** The H_2O_2 adduct of $Bu_3P=O$, **2a** (0.250 g, 0.991 mmol, assuming one molecule of H_2O_2 per one phosphine oxide molecule), was placed into an NMR tube. **2a** was dissolved in 0.5 mL of C_6D_6 , and a capillary containing the neat standard $CIPPh_2$ was centered in the NMR tube. The ^{31}P NMR spectrum was recorded applying 32 scans. Subsequently the solution was transferred into a 20 mL vial, and an additional 0.5 mL of C_6D_6 was added. A 0.5 mL aliquot of this solution was placed in the NMR tube and measured as described above. This procedure was repeated ten additional times until a total volume of 6.0 mL was reached. Then 1.5 mL aliquots of C_6D_6 were added three times for greater dilution. The final volume of the mixture was then 10.5 mL.

Representative procedure for the synthesis of the phosphine oxides 1–5 from their H_2O_2 adducts 1a–5a using molecular sieves. The H_2O_2 adduct **2a** (3.751 g), obtained by treatment of Bu_3P (3.552 g, 17.56 mmol) with aqueous H_2O_2 as described above, was placed into a round bottom flask and dissolved in 150 mL of toluene. Then, a tea bag (obtained by removing the contents of a commercially available tea bag) was filled with 5 g of activated molecular sieves, closed by stapling and suspended in the middle of the flask and fully immersed in the solvent (Fig. 13). The solution underneath the tea bag was stirred vigorously at room temperature for 4 h. After retrieving the molecular sieves, the solvent was removed *in vacuo* to give **2** as a colorless powder (3.540 g, 16.21 mmol) in 92.3% yield with respect to the starting phosphine. At 60 °C this reaction is complete after 1 h. All phosphine oxides **1–5** were colorless crystalline solids, and they were characterized by ^{31}P NMR and IR spectroscopy, as well as their melting points (see Tables 1–3). For the sake of completeness, and because there are noticeable differences between the data of the phosphine oxides and their H_2O_2 adducts, the 1H and ^{13}C NMR data are included (see below, (c) in the experimental section).

Representative procedure for decomposition of 1a–5a to form 1–5 using wet silica. Toluene (30 mL) was combined with wet silica (0.995 g, no pre-conditioning) and **2a** (0.313 g, 1.240 mmol, assuming one molecule of H_2O_2 per one phosphine oxide molecules), dissolved in 20 mL of toluene, was added to the slurry *via* pipette with vigorous stirring. The mixture was stirred at RT for 18 h. After the silica had been allowed to settle down for 1 h, the supernatant was decanted. The solvent was removed *in vacuo* to give **2** as a colorless sticky solid (0.146 g, 53.9% yield). The silica was washed with CH_2Cl_2 (2 × 20 mL) to recover residual surface-adsorbed phosphine oxide **2** (0.089 g, 86.8% combined yield). The decomposition of the adduct **2a** to **2** was confirmed by ^{31}P NMR. The IR spectrum showed a significant amount of water remaining hydrogen-bonded to **2** (see results and discussion section).

Representative procedure for decomposition of 1a–5a to form 1–5 using pre-dried silica. The H_2O_2 adduct of $Bu_3P=O$ (**2a**, 0.537 g, 2.128 mmol assuming one molecule of H_2O_2 per one phosphine oxide molecules) was added to a slurry of dry silica (1.356 g) in toluene (30 mL) at RT. The sample was stirred overnight. An IR spectrum showed a significant amount of H_2O_2 remaining

in the material. Another 1.027 g of silica was added, and the slurry was stirred for a further 4 d. IR analysis proved that all H_2O_2 decomposed, and that the resulting water was quantitatively removed from the phosphine oxide. The supernatant was decanted, and the silica was washed with 20 mL of THF (more wash cycles would improve the yield)¹⁶ to recover residual surface-adsorbed **2**. The washes were combined and the solvent removed in vacuum to give **2** as a white polycrystalline solid (0.181 g, 39.0% overall yield).

Representative procedure for the decomposition of H_2O_2 in the adducts 1a–5a with heating. The H_2O_2 adduct of $\text{Bu}_3\text{P}=\text{O}$ (**2a**, 1.124 g) was placed in a Schlenk flask under nitrogen and dissolved in toluene (100 mL). Then the solution was heated to 90 °C for 18 h. After cooling to room temperature an aliquot (20 mL) was removed and placed in a separate Schlenk flask. The solvent was removed from this aliquot in vacuum, and a ^{31}P NMR spectrum showed that the H_2O_2 in the adduct **2a** was not completely decomposed. This result was confirmed by IR, which shows O–H stretching bands for H_2O and H_2O_2 bound to the phosphine oxide **2** (Fig. 10). The sample was redissolved in 20 mL of toluene and added to the original flask for further heating to 95 °C for 18 h. After this round of heating the H_2O_2 was entirely decomposed, but significant amounts of water remained bound to the phosphine oxide **2** as shown by IR. Sodium sulfate (*ca.* 2 g) was added to the solution, but this was ineffective in removing the residual water.

Representative procedure for decomposition of adducts with MnO_2 . The H_2O_2 adduct of $\text{Bu}_3\text{P}=\text{O}$ (**2a**, 0.110 g) was placed into a 20 mL vial and dissolved in 5 mL of toluene. When MnO_2 (0.101 g) was added, vigorous bubbling occurs due to the release of oxygen during the decomposition of H_2O_2 . The reaction mixture was stirred for 1 h at RT to complete the decomposition process. Then the mixture was filtered through a Pasteur pipette filled with silica gel to remove the MnO_2 . The latter was a fine black powder that is not entirely removable by filtration, as indicated by the dark color of the filtrate. The same result was obtained with filter paper while Celite improved the process slightly. Finally, the toluene was removed *in vacuo*, and the grey product was kept under nitrogen. ^{31}P NMR confirms the decomposition of the H_2O_2 in **2a**, leading to crude $\text{2}\cdot(\text{H}_2\text{O})_x$ (0.167 g).

Representative procedure for attempted decomposition of H_2O_2 adducts 1a–5a with Cu. The H_2O_2 adduct of $\text{Bu}_3\text{P}=\text{O}$ (**2a**, 0.110 g) was placed into an NMR tube and dissolved in 0.6 mL of C_6D_6 . Small copper pieces, cut from a copper wire (*ca.* 0.1 g overall), were added directly to the NMR tube. The solution was vigorously shaken for 0.5 h, then left at RT for 18 h with occasional shaking. After removal of the copper, the ^{31}P NMR spectrum of the solution showed that no decomposition of the H_2O_2 in **2a** had occurred. The same negative result was obtained when a solution of **2a** was heated to 40 °C for 18 h in the presence of copper pieces or when the mixture was stirred for one week at room temperature.

Representative procedure for measuring H_2O uptake of the phosphine oxides 1–5. Polycrystalline $\text{Bu}_3\text{P}=\text{O}$ (**2**) (1.160 g, 5.313 mmol) was placed on a watch glass and exposed to air. The combined mass of **2** and the watch glass was recorded in intervals of several minutes during the first hour to determine the uptake of H_2O gravimetrically. As H_2O was absorbed by **2**, the crystals became more “wet” in appearance and began to turn into an oil.

While the phosphine oxide **2** was exposed to air for a further 8 h, it completely transformed into the oil $\text{Bu}_3\text{P}=\text{O}\cdot(\text{H}_2\text{O})_{0.84}$ (1.240 g), and no mass increase was noted thereafter.

The result of this experiment is graphically displayed in Fig. 3, together with the similar data obtained for $\text{Me}_3\text{P}=\text{O}$ (**1**). For $\text{Oct}_3\text{P}=\text{O}$ (**3**), $\text{Cy}_3\text{P}=\text{O}$ (**4**), and $\text{Ph}_3\text{P}=\text{O}$ (**5**) no significant mass changes could be observed when they were exposed to humid air.

Representative procedure quantifying the loss of phosphine oxides 1–5 by adsorption on molecular sieves. The H_2O_2 adduct of $\text{Bu}_3\text{P}=\text{O}$ (**2a**, 1.010 g) was placed in a Schlenk flask and dissolved in 50 mL of toluene. A ^{31}P NMR spectrum of the solution (0.5 mL aliquot) was recorded to determine the mole percent of **2** (incorporated in **2a**) with respect to the standard ClPPh_2 in a capillary centered in the middle of the NMR tube (12.755 mole %). Molecular sieves (2.206 g) in a tea bag (commercially obtained tea bags are cut upen, stripped of their original contents, filled with the molecular sieves and sealed with staples, see Fig. 13) were then fully immersed in the solution, and the mixture was stirred at RT for 18 h. A ^{31}P NMR spectrum of the supernatant solution (0.5 mL aliquot) was again recorded, and the amount of **2** was 12.183 mol% as compared to the same standard ClPPh_2 . Therefore, 4.49 mol% of the phosphine oxide **2** had been lost from the solution by adsorption on the molecular sieves. This corresponded to a loss of 2.03 mol% of **2** per g of molecular sieves. The loss of the phosphine oxides **1** and **3–5** due to adsorption on the molecular sieves had been determined to be less than 2 mol% per g of molecular sieves under identical conditions.

(c) NMR data of the phosphine oxides and their H_2O_2 adducts

Trimethylphosphine oxide H_2O_2 adduct (1a). NMR (δ , CDCl_3), $^{31}\text{P}\{\text{H}\}$ 43.23 (s); ^1H 1.57 (d, $^2J(^{31}\text{P}-^1\text{H}) = 13.0$ Hz); $^{13}\text{C}\{\text{H}\}$ 17.56 (d, $^1J(^{31}\text{P}-^{13}\text{C}) = 70.1$ Hz).

Trimethylphosphine oxide (1). NMR (δ , C_6D_6), $^{31}\text{P}\{\text{H}\}$ 32.65 (s); ^1H 0.90 (d, $^2J(^{31}\text{P}-^1\text{H}) = 12.8$ Hz); $^{13}\text{C}\{\text{H}\}$ 17.99 (d, $^1J(^{31}\text{P}-^{13}\text{C}) = 69.0$ Hz).

NMR (δ , CDCl_3), $^{31}\text{P}\{\text{H}\}$ 38.79 (s); ^1H 1.51 (d, $^2J(^{31}\text{P}-^1\text{H}) = 12.8$ Hz); $^{13}\text{C}\{\text{H}\}$ 18.06 (d, $^1J(^{31}\text{P}-^{13}\text{C}) = 70.0$ Hz).

Tributylphosphine oxide H_2O_2 adduct (2a). NMR (δ , C_6D_6), $^{31}\text{P}\{\text{H}\}$ 51.12 (s); ^1H 1.47–1.34 (m, 12H, PCH_2CH_2), 1.22 (sextet, 6H, $^3J(^1\text{H}-^1\text{H}) = 7.2$ Hz, CH_2CH_3), 0.80 (t, 9H, $^3J(^1\text{H}-^1\text{H}) = 7.3$ Hz, CH_3); $^{13}\text{C}\{\text{H}\}$ 27.56 (d, $^1J(^{31}\text{P}-^{13}\text{C}) = 65.1$ Hz, PCH_2), 24.51 (d, $^3J(^{31}\text{P}-^{13}\text{C}) = 14.0$ Hz, CH_2CH_3), 24.00 (d, $^2J(^{31}\text{P}-^{13}\text{C}) = 3.8$ Hz, PCH_2CH_2), 13.83 (s, CH_3).

NMR (δ , CDCl_3), $^{31}\text{P}\{\text{H}\}$ 52.50 (s); ^1H 1.64–1.56 (m, 6H, PCH_2), 1.47–1.38 (m, 6H, PCH_2CH_2), 1.32 (sextet, 6H, $^3J(^1\text{H}-^1\text{H}) = 7.2$ Hz, CH_2CH_3), 0.82 (t, 9H, $^3J(^1\text{H}-^1\text{H}) = 7.3$ Hz, CH_3); $^{13}\text{C}\{\text{H}\}$ 26.90 (d, $^1J(^{31}\text{P}-^{13}\text{C}) = 65.2$ Hz, PCH_2), 23.92 (d, $^3J(^{31}\text{P}-^{13}\text{C}) = 14.4$ Hz, CH_2CH_3), 23.32 (d, $^2J(^{31}\text{P}-^{13}\text{C}) = 3.9$ Hz, PCH_2CH_2), 13.29 (s, CH_3).

Tributylphosphine oxide (2). NMR (δ , C_6D_6), $^{31}\text{P}\{\text{H}\}$ 43.66 (s); ^1H 1.49–1.38 (m, 6H, PCH_2CH_2), 1.36–1.29 (m, 6H, PCH_2), 1.23 (sextet, 6H, $^3J(^1\text{H}-^1\text{H}) = 7.3$ Hz, CH_2CH_3), 0.81 (t, 9H, $^3J(^1\text{H}-^1\text{H}) = 7.3$ Hz, CH_3); $^{13}\text{C}\{\text{H}\}$ 28.13 (d, $^1J(^{31}\text{P}-^{13}\text{C}) = 65.0$ Hz, PCH_2), 24.53 (d, $^3J(^{31}\text{P}-^{13}\text{C}) = 13.6$ Hz, CH_2CH_3), 24.17 (d, $^2J(^{31}\text{P}-^{13}\text{C}) = 3.8$ Hz, PCH_2CH_2), 13.82 (s, CH_3).

NMR (δ , CDCl₃), ³¹P{¹H} 48.57 (s); ¹H 1.69–1.64 (m, 6H, PCH₂), 1.57–1.49 (m, 6H, PCH₂CH₂), 1.42 (sextet, 6H, ³J(¹H–¹H) = 7.2 Hz, CH₂CH₃), 0.92 (t, 9H, ³J(¹H–¹H) = 7.3 Hz, CH₃); ¹³C{¹H} 27.63 (d, ¹J(³¹P–¹³C) = 65.0 Hz, PCH₂), 24.28 (d, ³J(³¹P–¹³C) = 14.2 Hz, CH₂CH₃), 23.75 (d, ²J(³¹P–¹³C) = 3.9 Hz, PCH₂CH₂), 13.60 (s, CH₃).

Trioctylphosphine oxide H₂O₂ adduct (3a). NMR (δ , C₆D₆), ³¹P{¹H} 48.60 (s); ¹H 1.52–1.37 (m, 12H, PCH₂CH₂), 1.28–1.12 (m, 30H, CH₂CH₃), 0.88 (t, 9H, ³J(¹H–¹H) = 7.2 Hz, CH₃); ¹³C{¹H} 32.29 (s, CH₂CH₂CH₃), 31.58 (d, ³J(³¹P–¹³C) = 13.6 Hz, P(CH₂)₂CH₂), 29.62 (s, P(CH₂)₃CH₂)_‡, 29.59 (s, P(CH₂)₄CH₂)_‡, 28.08 (d, ¹J(³¹P–¹³C) = 64.8 Hz, PCH₂), 23.09 (s, CH₂CH₃), 22.10 (d, ²J(³¹P–¹³C) = 3.7 Hz, PCH₂CH₂), 14.36 (s, CH₃).

NMR (δ , CDCl₃), ³¹P{¹H} 50.01 (s); ¹H 1.71–1.62 (m, 6H, PCH₂), 1.57–1.47 (m, 6H, PCH₂CH₂), 1.41–1.32 (m, 6H, PCH₂CH₂CH₂), 1.32–1.28 (m, 24H, (CH₂)₄CH₃), 0.86 (t, 9H, ³J(¹H–¹H) = 7.2 Hz, CH₃); ¹³C{¹H} 31.61 (s, CH₂CH₂CH₃), 30.98 (d, ³J(³¹P–¹³C) = 13.8 Hz, P(CH₂)₂CH₂), 28.90 (s, P(CH₂)₃CH₂)_‡, 28.88 (s, P(CH₂)₄CH₂)_‡, 27.57 (d, ¹J(³¹P–¹³C) = 64.6 Hz, PCH₂), 22.44 (s, CH₂CH₃), 21.46 (d, ²J(³¹P–¹³C) = 2.7 Hz, PCH₂CH₂), 13.87 (s, CH₃).

Trioctylphosphine oxide (3). NMR (δ , C₆D₆), ³¹P{¹H} 43.93 (s); ¹H 1.57–1.48 (m, 6H, PCH₂CH₂), 1.44–1.37 (m, 6H, PCH₂), 1.33–1.19 (br m, 30H, (CH₂)₅CH₃), 0.91 (t, 9H, ³J(¹H–¹H) = 7.1 Hz, CH₃); ¹³C{¹H} 32.24 (s, CH₂CH₂CH₃), 31.57 (d, ³J(³¹P–¹³C) = 13.1 Hz, P(CH₂)₂CH₂), 29.58 (s, P(CH₂)₃CH₂)_‡, 29.57 (s, P(CH₂)₄CH₂)_‡, 28.49 (d, ¹J(³¹P–¹³C) = 64.6 Hz, PCH₂), 23.06 (s, CH₂CH₃), 22.21 (d, ²J(³¹P–¹³C) = 3.8 Hz, PCH₂CH₂), 14.35 (s, CH₃).

NMR (δ , CDCl₃), ³¹P{¹H} 48.48 (s); ¹H 1.67–1.59 (m, 6H, PCH₂), 1.58–1.48 (m, 6H, PCH₂CH₂), 1.40–1.32 (m, 6H, PCH₂CH₂CH₂), 1.32–1.18 (br m, 24H, (CH₂)₄CH₃), 0.85 (t, 9H, ³J(¹H–¹H) = 7.1 Hz, CH₃); ¹³C{¹H} 31.78 (s, CH₂CH₂CH₃), 31.39 (d, ³J(³¹P–¹³C) = 13.6 Hz, P(CH₂)₂CH₂), 29.09 (s, P(CH₂)₃CH₂)_‡, 29.04 (s, P(CH₂)₄CH₂)_‡, 27.95 (d, ¹J(³¹P–¹³C) = 65.0 Hz, PCH₂), 22.61 (s, CH₂CH₃), 21.70 (d, ²J(³¹P–¹³C) = 3.7 Hz, PCH₂CH₂), 14.06 (s, CH₃).

Tricyclohexylphosphine oxide H₂O₂ adduct (4a). NMR (δ , C₆D₆), ³¹P{¹H} 50.28 (s); ¹H 1.87 (br d, 6H, ²J(¹H_{eq}–¹H_{ax}) = 12.8 Hz, PCHCH_{eq}), 1.74 (dtt, 3H, ²J(³¹P–¹H_{ax}) = 11.7 Hz, ³J(¹H_{ax}–¹H_{ax}) = 12.6 Hz, ³J(¹H_{ax}–¹H_{eq}) = 3.0 Hz, PCH_{ax}), 1.67–1.61 (m, 6H, PCHCH₂CH_{eq}), 1.56–1.51 (m, 3H, PCH(CH₂)₂CH_{eq}), 1.44–1.33 (m, 6H, PCHCH_{ax}), 1.12–1.00 (m, 9H, PCHCH₂CH_{ax}CH_{ax}); ¹³C{¹H} 35.41 (d, ¹J(³¹P–¹³C) = 61.0 Hz, PCH), 27.11 (d, ³J(³¹P–¹³C) = 11.9 Hz, PCHCH₂CH₂), 26.50 (d, ²J(³¹P–¹³C) = 2.9 Hz, PCHCH₂), 26.39 (d, ⁴J(³¹P–¹³C) = 1.3 Hz, PCH(CH₂)₂CH₂).}}}}}}

NMR (δ , CDCl₃), ³¹P{¹H} 51.53 (s); ¹H 1.94–1.78 (m, 15H, PCH_{ax}CH_{eq}CH_{eq}), 1.74–1.67 (m, 3H, PCH(CH₂)₂CH_{eq}), 1.47–1.35 (m, 6H, PCHCH_{ax}), 1.29–1.17 (m, 9H, PCHCH₂CH_{ax}CH_{ax}); ¹³C{¹H} 35.19 (d, ¹J(³¹P–¹³C) = 60.8 Hz, PCH), 26.87 (d, ³J(³¹P–¹³C) = 11.7 Hz, PCHCH₂CH₂), 26.23 (d, ²J(³¹P–¹³C) = 2.9 Hz, PCHCH₂), 26.08 (d, ⁴J(³¹P–¹³C) = 1.4 Hz, PCH(CH₂)₂CH₂).

Tricyclohexylphosphine oxide (4). NMR (δ , C₆D₆), ³¹P{¹H} 46.31 (s); ¹H 1.91 (br d, 6H, ²J(¹H_{eq}–¹H_{ax}) = 12.7 Hz, PCHCH_{eq}), 1.73 (dtt, 3H, ²J(³¹P–¹H_{ax}) = 11.5 Hz, ³J(¹H_{ax}–¹H_{ax}) =}}}}}

12.5 Hz, ³J(¹H_{ax}–¹H_{eq}) = 3.0 Hz, PCH_{ax}), 1.68–1.62 (m, 6H, PCHCH₂CH_{eq}), 1.57–1.52 (m, 3H, PCH(CH₂)₂CH_{eq}), 1.46–1.35 (m, 6H, PCHCH_{ax}), 1.13–1.00 (m, 9H, PCHCH₂CH_{ax}CH_{ax}); ¹³C{¹H} 35.49 (d, ¹J(³¹P–¹³C) = 61.0 Hz, PCH), 27.13 (d, ³J(³¹P–¹³C) = 11.6 Hz, PCHCH₂CH₂), 26.57 (d, ²J(³¹P–¹³C) = 2.9 Hz, PCHCH₂), 26.42 (d, ⁴J(³¹P–¹³C) = 1.3 Hz, PCH(CH₂)₂CH₂).}}

NMR (δ , CDCl₃), ³¹P{¹H} 49.91 (s); ¹H 1.91 (br d, 6H, ²J(¹H–¹H) = 12.8 Hz, PCHCH_{eq}), 1.88–1.79 (m, 9H, PCH_{ax}CH₂CH_{eq}), 1.75–1.68 (m, 3H, PCH(CH₂)₂CH_{eq}), 1.48–1.36 (m, 6H, PCHCH_{ax}), 1.30–1.18 (m, 9H, PCHCH₂CH_{ax}CH_{ax}); ¹³C{¹H} 35.37 (d, ¹J(³¹P–¹³C) = 60.8 Hz, PCH), 26.93 (d, ³J(³¹P–¹³C) = 11.6 Hz, PCHCH₂CH₂), 26.34 (d, ²J(³¹P–¹³C) = 2.9 Hz, PCHCH₂), 26.14 (d, ⁴J(³¹P–¹³C) = 1.4 Hz, PCH(CH₂)₂CH₂).

Triphenylphosphine oxide H₂O₂ adduct (5a). NMR (δ , C₆D₆), ³¹P{¹H} 27.52 (s); ¹H 7.75–7.69 (m, 6H, H_o), 7.06–6.96 (m, 9H, H_m, H_p); ¹³C{¹H} 134.12 (d, ¹J(³¹P–¹³C) = 103.0 Hz, C_i), 132.40 (d, ²J(³¹P–¹³C) = 9.7 Hz, C_o), 131.61 (d, ⁴J(³¹P–¹³C) = 2.8 Hz, C_p), 128.55 (d, ³J(³¹P–¹³C) = 12.1 Hz, C_m).

NMR (δ , CDCl₃), ³¹P{¹H} 30.15 (s); ¹H 7.69–7.64 (m, 6H, H_o), 7.57–7.52 (m, 3H, H_p), 7.48–7.44 (m, 6H, H_m); ¹³C{¹H} 132.31 (d, ¹J(³¹P–¹³C) = 102.8 Hz, C_i), 132.06 (d, ²J(³¹P–¹³C) = 10.0 Hz, C_o), 131.96 (d, ⁴J(³¹P–¹³C) = 2.8 Hz, C_p), 128.49 (d, ³J(³¹P–¹³C) = 12.3 Hz, C_m).

Triphenylphosphine oxide (5). NMR (δ , C₆D₆), ³¹P{¹H} 25.16 (s); ¹H 7.77–7.71 (m, 6H, H_o), 7.06–6.96 (m, 9H, H_m, H_p); ¹³C{¹H} 134.00 (d, ¹J(³¹P–¹³C) = 102.6 Hz, C_i), 132.04 (d, ²J(³¹P–¹³C) = 9.7 Hz, C_o), 131.17 (d, ⁴J(³¹P–¹³C) = 2.7 Hz, C_p), 128.15 (d, ³J(³¹P–¹³C) = 11.9 Hz, C_m).

NMR (δ , CDCl₃), ³¹P{¹H} 29.10 (s); ¹H 7.70–7.64 (m, 6H, H_o), 7.57–7.52 (m, 3H, H_p), 7.49–7.43 (m, 6H, H_m); ¹³C{¹H} 132.54 (d, ¹J(³¹P–¹³C) = 103.4 Hz, C_i), 132.07 (d, ²J(³¹P–¹³C) = 9.9 Hz, C_o), 131.89 (d, ⁴J(³¹P–¹³C) = 2.8 Hz, C_p), 128.46 (d, ³J(³¹P–¹³C) = 12.1 Hz, C_m).

(d) Crystallography

General procedure. Data were collected using a BRUKER APEX2 X-ray diffractometer. Cell parameters were obtained from 60 frames using a 0.5° scan and refined using the number of reflections given in sections A and B below. Integrated intensity information for each reflection was obtained by reduction of the data frames with the program APEX2.⁴⁰ Lorentz, polarization, crystal decay effects, and absorption corrections⁴¹ were applied. The space group was determined from systematic reflection conditions and statistical tests. The structure was solved by direct methods using SHELXTL (SHELXS) and refined (weighted least squares refinement on *F*²) using SHELXL-97.⁴² Non-hydrogen atoms were refined with anisotropic thermal parameters. The parameters were refined by weighted least squares refinement on *F*² to convergence.⁴²

A. A nearly saturated toluene solution of **2** was sealed in a vial under N₂ and kept first in a refrigerator (2 °C, 1 h) and then a freezer (–17 °C, 12 h). The colorless needles were directly mounted from the warmed sample. Hydrogen atoms were placed in idealized positions and were refined using a riding model.

Crystal data: C₁₂H₂₇OP, *M*_r = 218.31, monoclinic, space group *P*2₁/*c*, *T* = 150(2)K, *a* = 9.326(6), *b* = 15.281(10), *c* = 10.136(7) Å, α = 90°, β = 100.548(15)°, γ = 90°, *V* = 1420.1(16) Å³, *Z* = 4,

‡ assignments are interchangeable

$D_c = 1.021 \text{ g cm}^{-3}$, $F_{000} = 488$, θ range for data collection 2.22° to 27.61° , 15 057 reflections collected, independent reflections 3264 ($R_{\text{int}} = 0.0594$). Final $\text{Goof} = 1.062$, R indices based on reflections with $I > 2\sigma(I)$ (refinement on F^2) $R_1 = 0.0595$, $wR_2 = 0.1490$, R indices (all data) $R_1 = 0.0885$, $wR_2 = 0.1788$.

B. A toluene solution of **4a** was sealed in a vial under N_2 and kept first in a refrigerator (2°C , 12 h) and then a freezer (-17°C , 2 d). The colorless blocks, which dissolved upon warming, were directly mounted from the cold sample. Carbon-bound hydrogen atoms were placed in idealized positions. Oxygen-bound hydrogen atoms were located from the difference Fourier map and refined using a riding model.

Crystal data: $\text{C}_{18}\text{H}_{35}\text{O}_3\text{P}$, $M_r = 330.43$, triclinic, space group $P\bar{1}$, $T = 110(2)\text{K}$, $a = 8.579(2)$, $b = 9.584(3)$, $c = 12.260(3) \text{ \AA}$, $\alpha = 95.445(3)^\circ$, $\beta = 97.065(3)^\circ$, $\gamma = 112.824(3)^\circ$, $V = 910.8(4) \text{ \AA}^3$, $Z = 2$, $D_c = 1.205 \text{ g cm}^{-3}$, $F_{000} = 364$, θ range for data collection 1.69° to 27.48° , 10409 reflections collected, 4067 independent reflections ($R_{\text{int}} = 0.0169$). Final $\text{Goof} = 1.044$, R indices based on reflections with $[I > 2\sigma(I)]$ (refinement on F^2) $R_1 = 0.0327$, $wR_2 = 0.0843$, R indices (all data) $R_1 = 0.0376$, $wR_2 = 0.0880$.

Acknowledgements

This material is based upon work supported by the National Science Foundation under CHE-0911207, CHE-0719267, and CHE-0840464. We thank The Welch Foundation (A-1706) for financial support, the ACS Division of Inorganic Chemistry, the Texas A&M Office of Graduate Studies, the NSF LSAMP Bridge to Doctorate program, and the NSF Graduate Research Program (C. R. Hilliard) for fellowships.

Notes and references

- (a) J. A. Gladysz, Ed., *Recoverable Catalysts and Reagents*, Special Issue of *Chem. Rev.*, 2002, **102**; (b) J. Blümel, *Coord. Chem. Rev.*, 2008, **252**, 2410–2423; (c) F. R. Hartley, *Supported Metal Complexes*, D. Reidel Publ. Co., Dordrecht, The Netherlands, 1985; (d) D. E. DeVos, I. F. J. Vankelecom and P. A. Jacobs, ed., *Chiral Catalyst Immobilization and Recycling*, Wiley-VCH, Weinheim, 2000; (e) G. Rothenberg, *Catalysis: Concepts and Green Applications*, Wiley-VCH, Weinheim, 2008; (f) P. Barbaro and F. Liguori, ed., *Heterogenized Homogeneous Catalysts for Fine Chemicals Production*, Springer Science and Business Media, Heidelberg, 2010.
- (a) J. Guenther, J. Reibenspies and J. Blümel, *Adv. Synth. Catal.*, 2011, **353**, 443–460; (b) T. Posset, J. Guenther, J. Pope, T. Oeser and J. Blümel, *Chem. Commun.*, 2011, **47**, 2059–2061; (c) B. Beele, J. Guenther, M. Perera, M. Stach, T. Oeser and J. Blümel, *New J. Chem.*, 2010, **34**, 2729–2731.
- (a) J. Boutagy and R. Thomas, *Chem. Rev.*, 1974, **74**, 87–99; (b) C. J. O'Brien, J. L. Tellez, Z. S. Nixon, L. J. Kang, A. L. Carter, S. R. Kunkel, K. C. Przeworski and G. A. Chass, *Angew. Chem., Int. Ed.*, 2009, **48**, 6836–6839.
- Y. G. Gololobov, I. N. Zhmurarova and L. F. Kasukhin, *Tetrahedron*, 1981, **37**, 437–472.
- R. Appel, *Angew. Chem., Int. Ed. Engl.*, 1975, **14**, 801–811.
- (a) T. E. Barder and S. L. Buchwald, *J. Am. Chem. Soc.*, 2007, **129**, 5096–5101; (b) S. A. Buckler, *J. Am. Chem. Soc.*, 1962, **84**, 3093–3097; (c) H. D. Burkett, W. E. Hill and S. D. Worley, *Phosphorus Sulfur Relat. Elem.*, 1984, **20**, 169–172.
- S. Hayashi, *Anal. Sci.*, 2009, **25**, 133–136.
- M. A. Beckett, D. S. Brassington, M. E. Light and M. B. Hursthouse, *J. Chem. Soc., Dalton Trans.*, 2001, 1768–1772.
- (a) R. D. Temple, Y. Tsuno and J. E. Leffler, *J. Org. Chem.*, 1963, **28**, 2495; (b) D. B. Copley, F. Fairbrother, J. R. Miller and A. Thompson, *Proc. Chem. Soc., London*, 1964, 300–301; (c) D. Thierbach, F. Huber and H. Preut, *Acta Crystallogr., Sect. B: Struct. Crystallogr. Cryst.*

- Chem.*, 1980, **36**, 974–977; (d) A. S. Kende, P. Delair and B. E. Blass, *Tetrahedron Lett.*, 1994, **35**, 8123–8126.
- (a) J. Blümel, *Inorg. Chem.*, 1994, **33**, 5050–5058; (b) Y. Yang, B. Beele and J. Blümel, *J. Am. Chem. Soc.*, 2008, **130**, 3771–3773; (c) J. Sommer, Y. Yang, D. Rambow and J. Blümel, *Inorg. Chem.*, 2004, **43**, 7561–7563; (d) T. Posset, F. Rominger and J. Blümel, *Chem. Mater.*, 2005, **17**, 586–595.
- (a) S. Hayashi, *Chem. Lett.*, 2009, **38**, 960–961; (b) R. Yerushalmi, J. C. Ho, Z. Fan and A. Javey, *Angew. Chem., Int. Ed.*, 2008, **47**, 4440–4442; (c) B. Alonso, I. Klur and D. Massiot, *Chem. Commun.*, 2002, 804–805; (d) L. Baltusis, J. S. Frye and G. E. Maciel, *J. Am. Chem. Soc.*, 1986, **108**, 7119–7120; (e) H.-M. Kao, P.-C. Chang, Y.-W. Liao, L.-P. Lee and C.-H. Chien, *Microporous Mesoporous Mater.*, 2008, **114**, 352–364; (f) J. Kříž, J. Dybal, E. Makrlík, J. Budka and Petr Vaňura, *J. Phys. Chem. A*, 2009, **113**, 5896–5905.
- (a) V. W. L. Ng, M. K. Taylor, L. M. R. Hill, J. M. White and C. G. Young, *Eur. J. Inorg. Chem.*, 2010, 3261–3269; (b) W. Tsai, Y.-H. Liu, S.-M. Peng and S.-T. Liu, *J. Organomet. Chem.*, 2005, **690**, 415–421.
- (a) L. Li, Z. Wang, X. Song and S. Sun, *Spectrochim. Acta, Part A*, 2009, **72**, 816–818; (b) M. T. Ben Dhia, M. A. M. K. Sanhoury, L. C. Owono Owono and M. R. Khaddar, *J. Mol. Struct.*, 2008, **892**, 103–109; (c) E. I. Toliş, K. A. Vallianatou, F. A. Andreadaki and I. D. Kostas, *Appl. Organomet. Chem.*, 2006, **20**, 335–337.
- (a) C. Popovici, I. Fernandez, P. Ona-Burgos, L. Roces, S. Garcia-Granda and F. L. Ortiz, *Dalton Trans.*, 2011, **40**, 6691–6703; (b) K. Miyata, Y. Hasegawa, Y. Kuramochi, T. Nakagawa, T. Yokoo and T. Kawai, *Eur. J. Inorg. Chem.*, 2009, 4777–4785.
- (a) L. Ackermann, S. Barfüßer, C. Kornhaas and A. R. Kapdi, *Org. Lett.*, 2011, **13**, 3082–3085; (b) L. Ackermann, A. R. Kapdi and C. Schulzke, *Org. Lett.*, 2010, **12**, 2298–2301.
- C. Hilliard, J. A. Gladysz and J. Blümel, *Chem. Mater.*, 2011, in preparation.
- M. M. Rauhut and H. A. Currier, *J. Org. Chem.*, 1961, **26**, 4626–4628.
- (a) W. Peng and J. M. Shreeve, *J. Fluorine Chem.*, 2005, **126**, 1054–1056; (b) D. Macikenas, E. Skrzypczak-Jankun and J. D. Protasiewicz, *J. Am. Chem. Soc.*, 1999, **121**, 7164–7165; (c) S. Porcel, G. Bouhadir, N. Saffon, L. Maron and D. Bourissou, *Angew. Chem., Int. Ed.*, 2010, **49**, 6186–6189; (d) G. C. Tucci, J. P. Donahue and R. H. Holm, *Inorg. Chem.*, 1998, **37**, 1602–1608; (e) J. M. Berg and R. H. Holm, *J. Am. Chem. Soc.*, 1985, **107**, 925–932.
- (a) T. M. Duncan, *A Compilation of Chemical Shift Anisotropies*, Farragut Press, Chicago, IL, 1990; (b) C. A. Fyfe, *Solid-State NMR for Chemists*, C.F.C. Press, Guelph, Canada, 1983; (c) M. J. Duer, *Introduction to Solid-State NMR Spectroscopy*, Blackwell Publishing, Oxford, 2004; (d) S. Reinhard and J. Blümel, *Magn. Reson. Chem.*, 2003, **41**, 406–416; (e) J. Mason, Ed., *Multinuclear NMR*, Plenum Press, New York, London, 1987.
- J. Blümel, M. Herker, W. Hiller and F. H. Köhler, *Organometallics*, 1996, **15**, 3474–3476.
- (a) L. Bemis, H. C. Clark, J. A. Davies, C. A. Fyfe and R. E. Wasylshen, *J. Am. Chem. Soc.*, 1982, **104**, 438–445; (b) N. J. Clayden, C. M. Dobson, L.-Y. Lian and D. J. Smith, *J. Magn. Reson.*, 1986, **69**, 476–487; (c) J. B. Robert and L. Wiesenfeld, *Mol. Phys.*, 1981, **44**, 319–327.
- (a) A. L. Spek, *Acta Crystallogr., Sect. C: Cryst. Struct. Commun.*, 1987, **43**, 1233–1235; (b) C. P. Brock, W. B. Schweizer and J. D. Dunitz, *J. Am. Chem. Soc.*, 1985, **107**, 6964–6970.
- M. Bogza, T. Oeser and J. Blümel, *J. Organomet. Chem.*, 2005, **690**, 3383–3389.
- V. I. Alekseev, Yu. V. Gatilov, T. M. Polyanskaya, V. V. Bakakin, Yu. A. Dyadin and L. A. Gaponenko, *Zh. Strukt. Khim.*, 1982, **23**, 86–91.
- J. A. Davies, S. Dutremez and A. A. Pinkerton, *Inorg. Chem.*, 1991, **30**, 2380–2387.
- M. Mantina, A. C. Chamberlin, R. Valero, C. J. Cramer and D. G. Truhlar, *J. Phys. Chem. A*, 2009, **113**, 5806–5812. See Table 12.
- W. R. Busing and H. A. Levy, *J. Chem. Phys.*, 1965, **42**, 3054–3059.
- P. Larkin, *Infrared and Raman Spectroscopy, Principles and Spectral Interpretation*, Academic Press, Elsevier, 2011.
- (a) L. W. Daasch and D. C. Smith, *J. Chem. Phys.*, 1951, **19**, 22–25; (b) G. Aksnes and L. J. Brudvik, *Acta Chem. Scand.*, 1963, **17**, 1616–1622; (c) W. Schneider, W. Thiel and A. Komornicki, *J. Phys. Chem.*, 1988, **92**, 5611–5619.
- G. V. Howell and R. L. Williams, *J. Chem. Soc. A*, 1968, 117–118.
- M. A. Hasnat, M. M. Rahman, S. M. Borhanuddin, A. Siddiqua, N. M. Bhadur and M. R. Karim, *Catal. Commun.*, 2010, **12**, 286–291.

-
- 32 (a) R. K. Iler, *The Chemistry of Silica*, John Wiley, New York, 1979; (b) R. P. W. Scott, *Silica Gel and Bonded Phases*, John Wiley and Sons, New York, 1993.
- 33 A. B. Burg and W. E. McKee, *J. Am. Chem. Soc.*, 1951, **73**, 4590–4591.
- 34 L. I. Kudryavtseva, *Zh. Obs. Khim.*, 1990, **60**, 74–79.
- 35 N. G. Feshchenko, I. K. Mazepa, Zh. K. Gorbatenko, Yu. P. Mackovetskii, V. P. Kukhar and A. V. Kirsanov, *Zh. Obs. Khim.*, 1969, **39**, 1219–1223.
- 36 A. Burger and N. D. Dawson, *J. Chem. Soc.*, 1951, **16**, 1250–1254.
- 37 (a) C. Merckle and J. Blümel, *Chem. Mater.*, 2001, **13**, 3617–3623; (b) C. Merckle and J. Blümel, *Top. Catal.*, 2005, **34**, 5–15; (c) S. Reinhard, P. Soba, F. Rominger and J. Blümel, *Adv. Synth. Catal.*, 2003, **345**, 589–602.
- 38 T. Nishimura, T. Onoue, K. Ohe and S. Uemura, *J. Org. Chem.*, 1999, **64**, 6750–6755.
- 39 R. Fetouaki, A. Seifert, M. Bogza, T. Oeser and J. Blümel, *Inorg. Chim. Acta*, 2006, **359**, 4865–4873.
- 40 APEX2, Program for Data Collection on Area Detectors, BRUKER AXS Inc., 5465 East Cheryl Parkway, Madison, WI 53711-5373, USA.
- 41 G. M. Sheldrick, SADABS, Program for Absorption Correction of Area Detector Frames, BRUKER AXS Inc., 5465 East Cheryl Parkway, Madison, WI 53711-5373, USA.
- 42 G. M. Sheldrick, *Acta Crystallogr., Sect. A*, 2008, **64**, 112–122.